

Focus Through Motion: RGB-Event Collaborative Token Sparsification for Efficient Object Detection

Nan Yang*, Yang Wang*, Zhanwen Liu†, Yuchao Dai, Yang Liu, Xiangmo Zhao

Abstract—Existing RGB-Event detection methods process the low-information regions of both modalities (background in images and non-event regions in event data) uniformly during feature extraction and fusion, resulting in high computational costs and suboptimal performance. To mitigate the computational redundancy during feature extraction, researchers have respectively proposed token sparsification methods for the image and event modalities. However, these methods employ a fixed number or threshold for token selection, hindering the retention of informative tokens for samples with varying complexity. To achieve a better balance between accuracy and efficiency, we propose FocusMamba, which performs adaptive collaborative sparsification of multimodal features and efficiently integrates complementary information. Specifically, an Event-Guided Multimodal Sparsification (EGMS) strategy is designed to identify and adaptively discard low-information regions within each modality by leveraging scene content changes perceived by the event camera. Based on the sparsification results, a Cross-Modality Focus Fusion (CMFF) module is proposed to effectively capture and integrate complementary features from both modalities. Experiments on the DSEC-Det and PKU-DAVIS-SOD datasets demonstrate that the proposed method achieves superior performance in both accuracy and efficiency compared to existing methods. The code will be available at <https://github.com/Zzzzzzzzz/FocusMamba>.

Index Terms—RGB-Event fusion, object detection, token sparsification.

I. INTRODUCTION

OBJECT detection is fundamental to intelligent systems like autonomous driving and intelligent security [1]–[13]. In poor lighting (e.g., low-light and over-exposure) and fast motion scenes, the low dynamic range and frame rate of frame-based cameras cause low-quality images [14], [15], significantly degrading the performance of frame-based methods [16]–[23]. Recently, the advent of event cameras has provided a promising solution to this challenge. With the high temporal resolution and high dynamic range, the event camera exhibits stable imaging under challenging conditions [24]–[33]. However, they perform poorly in static or slow-motion scenes and cannot capture color and texture, which are critical

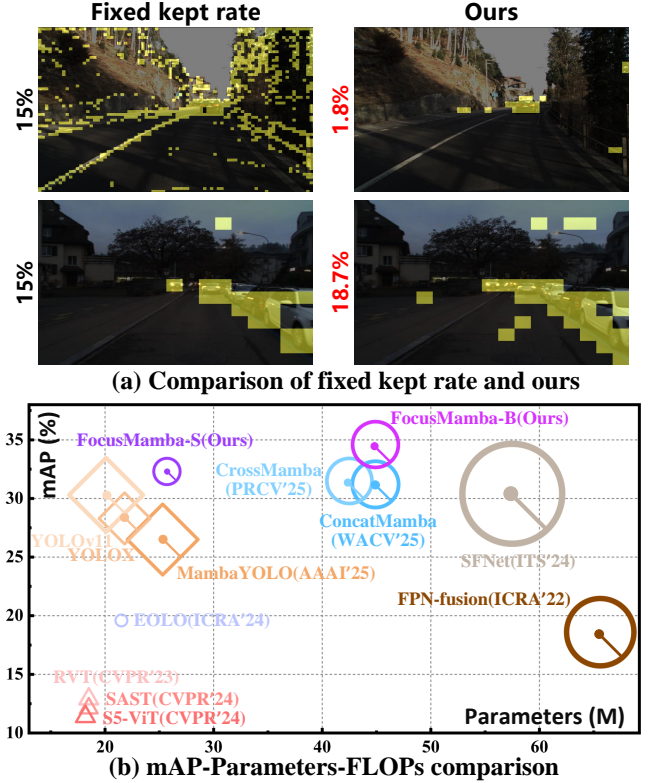


Fig. 1. (a) Comparison of token retention (yellow regions) between the fixed kept rate and our method. Our method can adaptively retain an appropriate number of tokens based on the scene complexity. (b) The mAP-Parameters-FLOPs comparison between state-of-the-art methods and our FocusMamba on the DSEC-Det dataset. The triangles, diamonds, and circles represent event-based, frame-based, and fusion-based methods, respectively, with the radius of each shape corresponding to its FLOPs. Our FocusMamba achieves an excellent balance between accuracy and efficiency.

for object detection [34]–[37]. Therefore, researchers [16], [34], [38]–[40] have proposed various fusion frameworks that combine the strengths of both cameras to improve robustness in challenging conditions.

Existing fusion frameworks independently extract representations for two modalities, followed by fusion modules to capture complementary information and improve representation discriminability. Although these methods outperform single-modal methods in accuracy, they inevitably reduce efficiency for two primary reasons. Firstly, during the representation extraction stage, they treat all information of both modalities equally, including crucial object areas and low-information regions (e.g., backgrounds in images and no-event regions in event data), neglecting the high redundancy of image

*Co-first author. †Corresponding author.

Nan Yang, Yang Wang, Zhanwen Liu and Xiangmo Zhao are with the School of Information Engineering, Chang'an University, Shaanxi, Xi'an 710000, China (e-mail: 2022024001@chd.edu.cn; ywang120@chd.edu.cn; zwliu@chd.edu.cn; xmzhao@chd.edu.cn).

Yuchao Dai is with the School of Electronics and Information, Northwestern Polytechnical University and Shaanxi Key Laboratory of Information Acquisition and Processing, Xi'an 710129, China (e-mail: daiyuchao@nwpu.edu.cn).

Yang Liu is with the School of Vehicle and Mobility, Tsinghua University, Beijing 100084, China, and also with State Key Laboratory of Intelligent Green Vehicle and Mobility, Beijing 100084, China (e-mail: thu_ets_lab@tsinghua.edu.cn).

backgrounds [41]–[43] and the spatial sparsity of event data [44], [45]. This leads to significant redundant computation and high computational costs. To address this issue, [41], [43], [46] and [44], [45] have respectively proposed token sparsification methods for the image and event modalities, discarding low-information regions from computation. However, their token selection strategy based on a fixed number or threshold neglects variations in sample content, which may result in under-sparsification of simple samples or over-sparsification of complex ones. As shown in Fig.1(a), at a 15% token retention rate, existing methods preserve excessive background content in the simple scene while failing to retain critical object information in the complex scene. Secondly, during the fusion stage, they apply attention mechanisms across all regions of both modality features to capture complementary relationships. However, this introduces background interference, leading to inaccurate perception of complementary regions and redundant computations.

To address the above issues, this paper proposes an RGB-Event collaborative sparsification object detection framework, FocusMamba, which aims to leverage the complementary characteristics of both modalities to perform adaptive sparsification of multimodal features and efficient integration of complementary features, achieving an excellent balance between accuracy and efficiency, as shown in Fig.1(b). First, we design an Event-Guided Multi-modality Sparsification (EGMS) strategy that adaptively discards low-information regions for each sample based on scene content changes perceived by the event camera, significantly reducing computational load, as shown in Fig.1(a). Specifically, a modality-specific statistical scoring method independently evaluates the importance of each modality’s tokens, maximizing the strengths of each modality. Subsequently, the event spatial ratio, which reflects the information content of objects, is utilized to adjust the score differentiation and threshold for each sample, generating sparsification maps that guide subsequent selective scanning and MLP for sparsification calculations. The sparsification maps effectively reflect the informative regions within each modality. The differences between these regions, arising from the distinct perceptual strengths of the modalities, highlight inter-modal complementary relationships. Building upon this, we propose a Cross-Modality Focus Fusion (CMFF) module that first efficiently captures complementary regions by perceiving the differences between the sparsification maps of the two modalities, and then performs fine-grained integration in the important areas preserved by EGMS, thereby suppressing background interference and reducing redundant computation. Overall, our contribution can be summarized as follows:

- (1) We propose the FocusMamba, which adaptively discards low-information regions for each sample, and focuses on the modeling and fusion of informative regions, achieving an ideal balance between accuracy and efficiency.
- (2) We design the EGMS strategy, which effectively identifies informative regions across modalities and adaptively retains them for each sample, significantly reducing computational costs.
- (3) We propose the CMFF module, which effectively perceives and finely integrates complementary features across

modalities based on sparsification results, thereby eliminating background interference.

(4) Comparison with 12 state-of-the-art methods (including event-only, RGB-only, and RGB-Event fusion) on the DSEC-Det and PKU-DAVIS-SOD datasets demonstrates that our method achieves the best performance, surpassing the second-best method SFNet by 4.2% and 0.8%, while requiring only 28.5% and 22.2% of its FLOPs, respectively.

II. RELATED WORK

This section provides an overview of RGB-Event fusion based detection methods, followed by a review of recent advancements in token sparsification and Vision Mamba.

RGB-Event fusion for object detection. Fusing RGB and event modalities is a crucial strategy for achieving high-performance detection in challenging conditions [16], [34], [38], [47], [48]. Among these fusion methods, the feature-level fusion strategy effectively utilizes the complementary strengths of both modalities, advancing rapidly. FPN-fusion [38] fuses features through concatenation. However, simple concatenation fails to differentiate the degradation levels of each modality and balance their contributions adaptively. To address this, SODFormer [34] perceives the degraded features of each modality through self-attention mechanisms to achieve adaptive fusion. SFNet [16] completes information lost in images by cross-modality global spatial similarity calculation. CAFR [48] achieves coarse-to-fine feature fusion through the cross-attention mechanism. However, they process the low-information regions of both modalities uniformly, resulting in high computational redundancy and inaccurate capture of complementary features.

Token sparsification. Recently, token sparsification methods have been proposed to improve the computational efficiency of the VLM (Vision-Language Model) domain, image classification, and object detection. It is noted that most sparsification methods in the VLM domain [49]–[53] rely on the ViT framework, text modality, or prior knowledge specific to VLM tasks, making them unsuitable for dense detection task and the Mamba framework. In image classification and object detection, they assign token importance scores using statistical methods (L2 norm [42], [46] and spatial-temporal continuity of events [45]) or by designing learnable modules for token importance prediction [43], [44], [54], [55] in token scoring stage. In token selection, they retain tokens by a fixed number [43], [46], [54] or threshold [42], [44], reducing the computational cost. However, the token selection strategy based on the fixed number or threshold has poor adaptability to diverse scenarios, hindering the retention of informative tokens for samples with varying complexity.

Vision Mamba. Compared to Transformers, Mamba [56] achieves a better balance between global modeling capability and computational efficiency. Specifically, Mamba introduces the input-dependent selective scanning mechanism to improve global modeling, while proposing a parallel scanning method to maintain linear complexity. Building on this, ViM [57] and VMamba [58] have developed the core Vision Mamba module to explore Mamba’s potential in visual tasks. Researchers

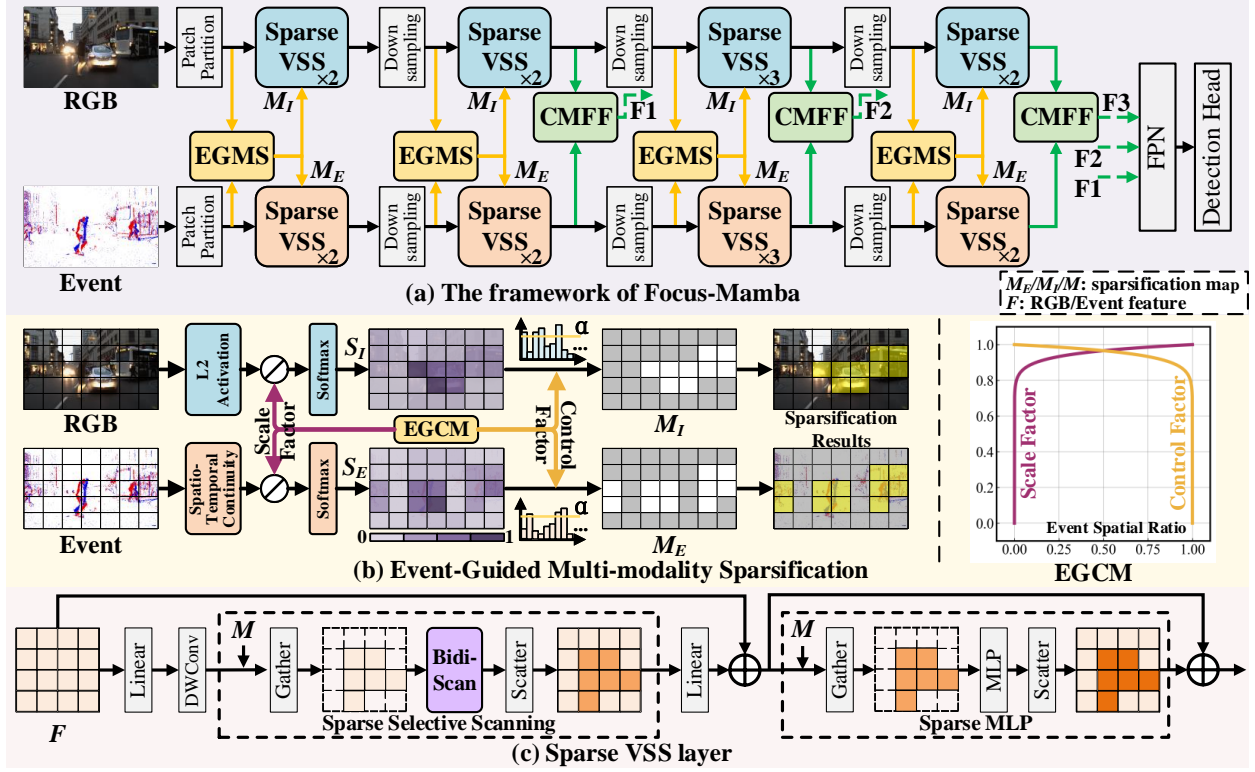


Fig. 2. **The architecture of FocusMamba.** The image and event tensors are first tokenized and then processed through four stages for multi-scale feature extraction. Before each stage, EGMS generates independent sparsification maps for both modalities to guide the sparsification operation. The CMFF module is applied in the final three stages to fuse the features of two modalities.

[59]–[66] have subsequently applied it to various visual tasks, demonstrating its advantages in the vision domain. However, Mamba lacks effective mechanisms for handling redundant image backgrounds and sparse event data, resulting in substantial redundant computations.

III. METHOD

A. The Overview of the FocusMamba

The framework of FocusMamba is illustrated in Fig.2(a). Initially, the event stream is converted into voxel tensor [67], and both the voxel tensor and RGB image are divided into patches for tokenization. Subsequently, the tokens from the two modalities are independently fed into two separate backbones, which process them through four stages to extract multi-scale features. In each stage, the Event-Guided Multi-modality Sparsification (EGMS) strategy, as shown in Fig.2(b), adaptively generates independent sparsification maps (M) for both modalities. These sparsification maps guide sparse selective scanning and sparse MLP in the subsequent Sparse VSS layer, significantly reducing computational costs, as shown in Fig.2(c). The Cross-Modality Focus Fusion (CMFF) module, as shown in Fig.4, is placed after the last three stages to effectively capture and integrate complementary features from both modalities under the guidance of the sparsification maps. The fused features are then fed into the FPN for multi-scale feature fusion. Finally, the YOLOv8 detection head outputs the detection results.

B. Event-Guided Multi-modality Sparsification

To adaptively discard low-information regions, we propose an Event-Guided Multi-modality Sparsification (EGMS) strategy, which consists of the scoring module and Event-Guided Control Mechanism (EGCM), as shown in Fig.2(b).

1) *Scoring Module:* Learnable scoring modules often fail to identify important tokens due to insufficient representation encoding in the early and middle layers [68], [69]. Therefore, we adopt more reliable statistical scoring methods [45], [46] to independently assess the importance of tokens in each modality, effectively identifying key information for each modality while maintaining minimal computational cost.

For the image modality, object regions are expected to be retained, while background regions are to be discarded. Therefore, L2 activation is employed as the scoring metric, as it effectively measures the feature response magnitude and importance of each token [42], [46], [70], enabling the identification of object regions. Specifically, the L2 norm $S_I \in \mathbb{R}^N$ of image tokens $X \in \mathbb{R}^{N \times C}$ is computed as:

$$S_{Ii} = \|X_i\|_2 = \sqrt{\sum_{j=1}^C X_{i,j}^2}, \quad (1)$$

where N is the token number, C is the feature dimension.

For the event modality, activity event regions are expected to be retained, while noise and non-event regions are to be discarded. Therefore, the spatiotemporal continuity of events [45] is used as the scoring metric, as it effectively identifies activity event regions based on the spatiotemporal distribution

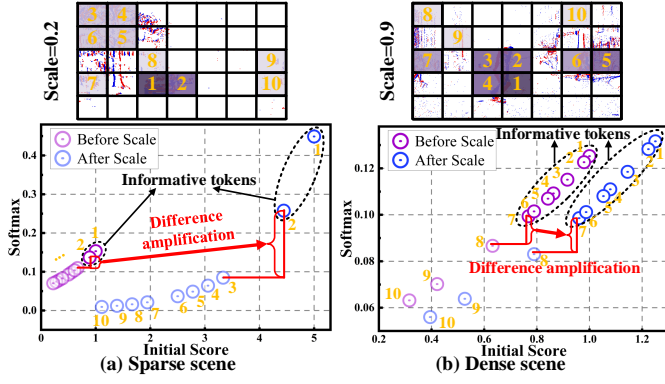


Fig. 3. We select 10 tokens from sparse and dense object-information scenes to show the score differences before and after scaling. The scale factor effectively amplifies the score differences, particularly in scenes with sparse object information.

differences between activity and noisy events. Specifically, given the event stream $\{(x_i, y_i, t_i, p_i)\}_{i=1}^K$, where (x_i, y_i) is the spatial coordinates, t_i is the timestamp, and $p_i \in \{-1, 1\}$ is the polarity. First, to identify temporally discontinuous noise events, the timestamps of events within the region corresponding to each token are accumulated to assess the temporal continuity, as follows:

$$S_{E_{x,y}}^T = \sum_{i, x_i=x, y_i=y} t_i, S_E^T = \text{Maxpooling}(S_{E_{x,y}}^T), \quad (2)$$

the kernel size and stride of MaxPooling are set to P , where P is the downsampling rate of the current stage. Subsequently, to further identify spatially isolated noise events and maintain complete structures for objects with sparse events, a Gaussian kernel is used to aggregate neighborhood information and assess the spatiotemporal continuity score, as follows:

$$S_E = \frac{\sum_{q \in \Omega} \left(\exp\left(-\frac{\|q-c\|^2}{2\sigma^2}\right) S_{E_q}^T \right)}{\sum_{q \in \Omega} \exp\left(-\frac{\|q-c\|^2}{2\sigma^2}\right)}, \quad (3)$$

where c is the center of the neighborhood Ω , $S_{E_q}^T$ is the value of the neighborhood q , and σ represents the variance.

2) *Event-Guided Control Mechanism*: After obtaining the token score maps S_I and S_E , a straightforward method for sparsification is to set a specific retention number or score threshold. However, this method has two limitations: (1) the initial scores from the scoring module lack sufficient contrast to distinguish informative tokens from low-information ones effectively; and (2) fixed retention numbers or thresholds fail to adapt to scene content variations, making it difficult to consistently preserve informative tokens across diverse scenarios. To address these challenges, we propose the Event-Guided Control Mechanism (EGCM), as shown in Fig.2(b), which adaptively regulates the score differences and selection thresholds based on the scene's sparsification level perceived by event camera, achieving sample-level multi-modal adaptive sparsification.

Moving objects frequently cause brightness changes along edges, continuously triggering events. Consequently, we can

estimate the spatial proportion of object information by computing the ratio r of pixels that trigger events to the total number of pixels. The ratio r can reflect the objects' information content and the scene's sparsification level to some extent. Based on this, we design the **scale factor** to amplify inter-token differences and the **control factor** to adaptively regulate the selection threshold.

Scale factor. The scale factor is integrated with softmax to amplify the score differences among tokens, as shown in Fig.3. The process is as follows:

$$\text{Scale} = r^{\frac{1}{\rho}}, \quad (4)$$

$$S_I = \text{softmax}\left(\frac{S_I}{\text{Scale}}\right), S_E = \text{softmax}\left(\frac{S_E}{\text{Scale}}\right), \quad (5)$$

ρ is a hyperparameter that regulates the sparsification process. In scenes with sparser object information, the scale value decreases, thereby amplifying token scores and increasing the disparity between them after the softmax operation. This facilitates the identification of informative tokens and the filtering of low-information ones.

Control factor. The control factor adaptively adjusts the sparsification threshold α according to the scene's sparsity level. The process is as follows:

$$\text{Control} = (1 - r)^{\frac{1}{\rho}}, \alpha = \frac{1}{N} \times \text{Control}. \quad (6)$$

In scenes with sparse object information, the limited number of informative tokens leads to higher softmax scores compared to dense scenes, as shown in the vertical axis of Fig.3. As a result, a higher threshold is required to filter out potential background regions. In contrast, scenes with dense object information contain more informative tokens, which results in lower softmax scores. Therefore, a lower threshold is necessary to prevent the loss of important information. Sparsification maps for both modalities are generated based on the threshold α :

$$M_I = \begin{cases} 1, & \text{if } S_I \geq \alpha, \\ 0, & \text{if } S_I < \alpha, \end{cases} \quad M_E = \begin{cases} 1, & \text{if } S_E \geq \alpha, \\ 0, & \text{if } S_E < \alpha. \end{cases} \quad (7)$$

The sparsification maps guide the sparsification operations in the subsequent layers of this stage.

C. Cross-Modality Focus Fusion

The regions retained in the sparsification maps primarily consist of high-quality information captured by the two modalities based on their respective perceptual strengths. For example, frame-based cameras can capture rich textures and static objects, while event cameras are capable of detecting objects under challenging exposure conditions. Due to the distinct perceptual advantages of the two modalities, their retained regions in the sparsification maps M_I and M_E are different, as shown in Fig.7(a). These differences highlight the inter-modal complementary relationship. Building on this, we propose the Cross-Modality Focus Fusion module, consisting of a Complementarity-Aware Enhancement (CAE) module and a Focused Interlaced Mamba (FI-Mamba) module, as shown in Fig.4. Guided by the sparsification maps, it accurately

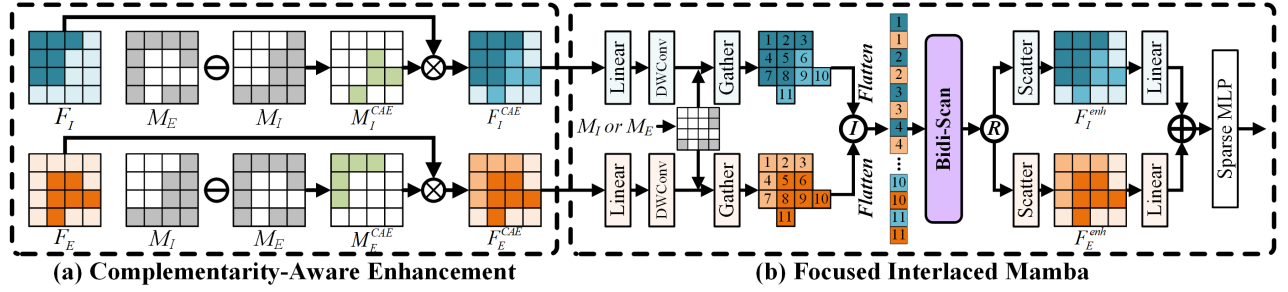


Fig. 4. **Cross-Modality Focus Fusion module.** Guided by the sparsification maps M_I and M_E , the CMFF module accurately captures and fully leverages the complementary features, eliminating background interference and reducing redundant computation.

captures and fully utilizes the complementary features of both modalities, while eliminating background interference.

To enhance the degraded regions in each modality (e.g., improperly exposed regions in RGB images and static object regions in event data) caused by perceptual limitations, we design the CAE module, as shown in Fig.4(a), which efficiently captures and utilizes inter-modal complementary regions. Specifically, the degradation regions of one modality relative to the other are perceived by performing the logical operation on the sparsification maps M_I and M_E , which then guides the enhancement of its features. Taking the image modality as an example, the process is as follows:

$$M_E - M_I = M_E \text{ xor } (M_E \text{ and } M_I), \quad (8)$$

$$M_I^{CAE} = \begin{cases} \beta, & \text{if } M_E - M_I = 1, \\ 1, & \text{if } M_E - M_I = 0, \end{cases} \quad (9)$$

$$F_I^{CAE} = M_I^{CAE} \cdot F_I, \quad (10)$$

where xor is the logical exclusive OR operation, and is the logical AND operation, \cdot denotes element-wise multiplication. M_I^{CAE} and β are the enhancement map and coefficient, respectively.

To further fully leverage the complementary advantages of both modalities, we propose the FI-Mamba, as shown in Fig.4(b), which integrates important tokens and simultaneously models long-range dependencies within and across modalities, facilitating refined feature fusion. Specifically, the features from two modalities are preprocessed using Linear and DW-Conv. Then, the important tokens are indicated based on the logical OR operation of the sparsification maps M_E and M_I :

$$M = M_I \text{ or } M_E, \quad (11)$$

where or is the logical OR operation. After obtaining M , the gather operation selects important tokens F_I' and F_E' from F_I^{CAE} and F_E^{CAE} based on the indices of non-zero elements in M , eliminating background interference while shortening the scan distance between crucial information. Subsequently, the interleaving operation flattens the selected tokens and alternately merges them into a new sequence. The sequence is input into the Bidi-Scan mechanism [58] to simultaneously model global dependencies both within and between modalities, enabling feature enhancement by leveraging information from both intra-modal and inter-modal sources. After that, the scatter operation maps the enhanced features F_I^{enh} and F_E^{enh}

back to the original feature map based on the indices of non-zero elements in M . Finally, the features are added and input into the Sparse MLP to further refine.

IV. EXPERIMENTS

This section begins with an overview of the experimental setup, followed by a comparative analysis of our method against state-of-the-art (SOTA) approaches. Then, ablation studies are conducted to validate the effectiveness of our method. Finally, we present visualization results to demonstrate the scene adaptability of our method.

A. Experimental Setup

Datasets. We conduct experiments on two datasets DSEC-Det [16] and PKU-DAVIS-SOD [34]. The DSEC-Det dataset contains challenging variable lighting conditions and high-quality manually annotated labels, providing more than 208k bounding boxes for 8 classes. There exist other versions of annotations for this dataset [2], [38], but they use automatic annotation methods, which result in poor label quality. Therefore, this work utilizes the more comprehensive and accurate annotations provided by [16]. The PKU-DAVIS-SOD dataset contains motion blur, low-light, and static scenes which is challenging for both modalities, and provides manual bounding boxes at 25 Hz for 3 classes, yielding more than 1080.1k labels. Considering that the data quality of the two modalities in the DSEC-Det dataset is higher and closer to real-world scenarios, this work chooses it to perform ablation studies.

Metrics. The COCO mAP [71] is used to evaluate the accuracy of the model. To assess model efficiency, we also report parameters, FLOPs, and runtime.

Implementation Details. To ensure a fair comparison, we follow prior methods [16], [34], [38] and sample the event stream using the inter-frame intervals of the RGB modality (50 ms for DSEC-Det and 40 ms for PKU-DAVIS-SOD). The image size is set to 640×640 for the DSEC-Det dataset and 416×416 for the PKU-DAVIS-SOD dataset during training and testing. We implemented the framework with Pytorch on Ubuntu 20.04 and trained it with 2 × NVIDIA-3090 and a batch size of 5 on each GPU. We adopted the Adam optimizer with the weight decay of 0.0005 and the learning rate of 0.01.

TABLE I

PERFORMANCE COMPARISON ON DSEC-DET AND PKU-DAVIS-SOD DATASETS. VALUES IN BRACKETS (·) INDICATE THE PERCENTAGE DECREASE IN FLOPS COMPARED TO THE BASELINE METHOD. THE BEST AND THE SUBOPTIMAL PERFORMANCES ARE MARKED IN **BOLD** AND UNDERLINE, RESPECTIVELY.

	Methods	Pub.&Yea.	DSEC-Det			PKU-DAVIS-SOD			
			mAP50/mAP	FLOPs	Runtime	mAP50/mAP	FLOPs	Runtime	Params
Event	SAST	CVPR'24	24.3/12.1	18.5G	18.8ms	48.7/24.5	6.2G	16.7ms	18.5M
	S5-ViT	CVPR'24	22.3/11.4	19.5G	12.3ms	46.6/23.3	7.3G	10.7ms	18.2M
	SMamba	AAAI'25	29.0/14.8	17.0G	26.1ms	53.0/27.1	5.2G	19.0ms	17.0M
RGB	YOLOX	arXiv'21	43.5/26.5	73.8G	15.3ms	57.5/30.6	31.1G	10.7ms	25.3M
	YOLOv11	arXiv'24	46.7/30.3	68.0G	16.2ms	58.0/30.9	44.2G	15.6ms	20.1M
	MambaYOLO	AAAI'25	44.1/28.3	47.2G	22.2ms	57.1/29.8	21.6G	21.0ms	21.8M
RGB-Event	FPN-fusion	ICRA'22	34.4/18.6	89.6G	30.8ms	36.6/19.5	49.7G	24.0ms	65.6M
	SODFormer	TPAMI'23	-	-	-	50.4/20.7	62.5G	39.7ms	82.0M
	EOLO	ICRA'24	33.9/19.6	13.7G	330.2ms	47.2/22.0	8.9G	326.4ms	21.5M
	SFNet	TITS'24	51.4/30.4	209G	44.8ms	59.6/31.9	135.9G	42.3ms	57.5M
	CAFR	ECCV'24	23.4/12.5	213.3G	117.7ms	52.0/26.0	63.5G	102.3ms	82.4M
	ACGR	CVPR'25	-	-	-	51.9/-	-G	16.8ms	41.4M
	SFNet*	TITS'24	25.0/12.7	54.2G	54.1ms	46.7/23.0	27.4G	50.9ms	38.3M
	CAFR*	ECCV'24	50.2/30.1	52.8G	50.5ms	58.0/30.8	27.1G	49.7ms	39.1M
	ConcatMamba	WACV'25	52.2/31.2	61.4G	55.3ms	58.3/31.1	30.4G	53.3ms	44.9M
	CrossMamba	PRCV'25	52.5/31.5	59.8G	53.4ms	58.3/31.2	29.3G	52.7ms	42.5M
	baseline-B	-	<u>52.5/32.6</u>	87.2G	61.0ms	<u>59.9/32.2</u>	42.9G	57.7ms	44.9M
	FocusMamba-B	-	55.3/34.6	60.8G (-30.3%)	54.7ms	60.6/32.7	30.2G (-29.6%)	53.5ms	44.9M
	FocusMamba-S	-	51.6/32.3	35.9G	53.4ms	59.7/32.2	17.8G	52.5ms	25.7M

B. Quantitative Results

We first compare our FocusMamba with recent SOTA object detection methods on DSEC-Det and PKU-DAVIS-SOD datasets, and then conduct comparative experiments with other sparsification methods to demonstrate the effectiveness of our EGMS strategy.

Comparison with SOTA object detection methods. We compare our method with recent SOTA methods, including three event-based methods: SAST [44], S5-ViT [72] and SMamba [45]; three frame-based methods: YOLOX [73], YOLOv11 [74] and MambaYOLO [75]; as well as six fusion-based methods: FPN-fusion [38], SODFormer [34], EOLO [40], SFNet [16], CAFR [48] and ACGR [76]. Furthermore, to compare with recent Mamba-based fusion methods and existing RGB-Event fusion modules, we introduce novel baselines by replacing our CMFF module with ConcatMamba [61], CrossMamba [64], and the fusion modules of SFNet and CAFR (referred to as SFNet* and CAFR*, respectively). And a baseline model without the EGMS strategy is established to evaluate the effectiveness of the proposed method. For a fair comparison with other methods, we train two models, a base model (FocusMamba-B) and a small model (FocusMamba-S) by adapting the channel dimensions in each stage.

As shown in Tab.I, our FocusMamba-B outperforms all other methods. For instance, compared to the SOTA fusion-based method SFNet on the two datasets, our method improves mAP by 4.2% and 0.8%, while requiring only 29.1% and 22.2% of SFNet's FLOPs, respectively. When compared to our constructed baseline, CrossMamba, our method achieves mAP improvements of 3.1% and 1.5%. Furthermore, after incorporating our sparsification strategy into baseline-B, FocusMamba-B achieves a 30.3% and 29.6% reduction in

TABLE II
PERFORMANCE COMPARED WITH SOTA TOKEN SPARSIFICATION METHODS ON DSEC-DET DATASET.

Methods	Pub.&Yea.	mAP50/mAP	FLOPs	Runtime
DivPrune	CVPR'25	51.1/30.2	68.0G	60.0ms
AS-ViT	IJCAI'23	53.7/33.0	65.3G	58.3ms
SparseViT	CVPR'23	52.8/32.9	69.7G	55.5ms
SViT	ECCV'22	53.8/32.8	68.5G	59.0ms
SAST	CVPR'24	53.2/32.6	63.2G	58.5ms
Ours	-	55.3/34.6	60.8G	54.7ms

FLOPs and a 10.3% and 7.3% decrease in runtime on the two datasets, respectively. This strategy also enables the model to focus on more critical regions, thereby improving detection accuracy. When compared to frame-based methods, our small model, FocusMamba-S, achieves higher accuracy and the lowest FLOPs while maintaining similar parameters. To be noted, FocusMamba's inference speed is currently limited by the early-stage development and inefficient hardware utilization of Mamba. Comparative experiments on the two datasets reveal that our method strikes an excellent balance between accuracy and efficiency through multimodal adaptive sparsification and effective integration of complementary features.

Comparison with other token sparsification methods. To further validate the effectiveness of our EGMS, we compare it with one available VLM domain method, DivPrune [77]; three image-modality methods: AS-ViT [42], SparseViT [46], and SViT [43]; and one event-modality method, SAST [44] on the DSEC-Det dataset. For fairness, all methods are adapted to sparsify both modalities independently while maintaining consistent architectural design.

As shown in Tab.II, the VLM-domain method DivPrune

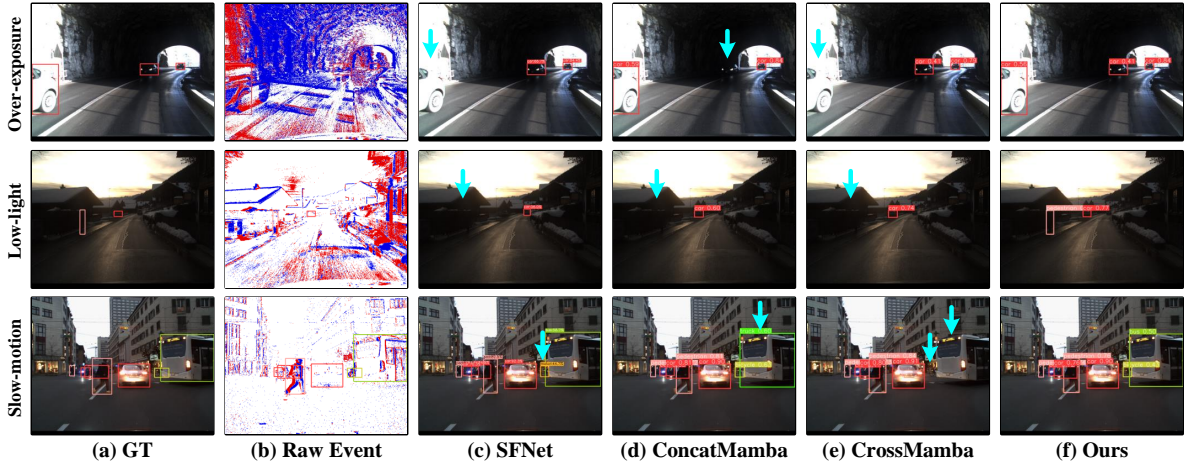


Fig. 5. Qualitative comparison with SFNet, ConcatMamba, and CrossMamba on the DSEC-Det dataset. We utilize blue arrows to mark the failed cases.

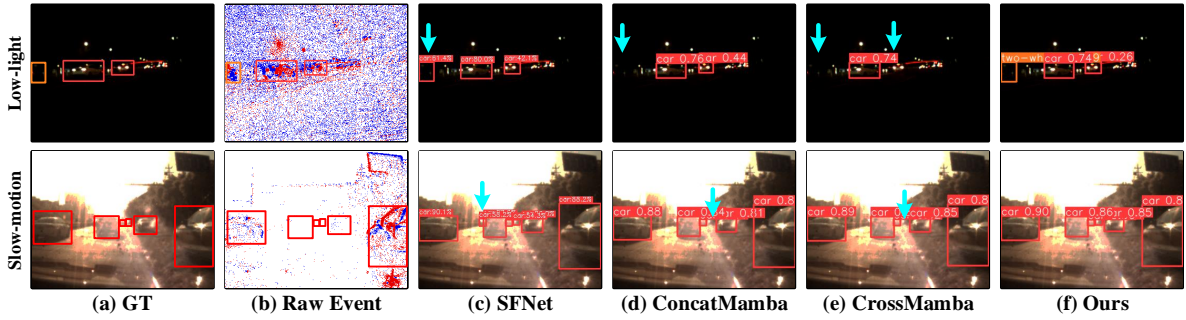


Fig. 6. Qualitative comparison with SFNet, ConcatMamba, and CrossMamba on the PKU-DAVIS-SOD dataset. We utilize blue arrows to mark the failed cases.

TABLE III
PERFORMANCE OF OUR COMPONENTS.

Method	mAP50/mAP	FLOPs	Params
- - -	50.3/31.6	81.5G	37.6M
+ EGMS	51.2/32.4	54.5G	37.6M
+ CAE	53.6/33.6	54.2G	37.6M
+ FI-Mamba	55.3/34.6	60.8G	44.9M

aims to retain the most diverse set of tokens rather than the object-relevant tokens required for detection tasks, resulting in the lowest performance. Despite utilizing L2 activation to improve scoring reliability, AS-ViT and SparseViT underperform due to their fixed threshold and pruning rate. SAST exhibits a degree of scene adaptability, achieving the lowest FLOPs among the compared methods. However, its adaptability is constrained by the unreliable learning-based scoring method and fixed threshold, resulting in limited accuracy. In contrast, our method leverages a reliable scoring mechanism specifically designed to align with the characteristics of modality signals, combined with an effective adaptive regulation strategy, achieving superior adaptive capability and detection accuracy.

C. Qualitative Comparison

We compare our FocusMamba with SFNet [16], ConcatMamba [61], and CrossMamba [64] on the DSEC-Det and

PKU-DAVIS-SOD datasets, as shown in Fig.5 and 6. Our FocusMamba demonstrates more robust detection performance in challenging scenarios (e.g., over-exposure, low-light, and slow-motion), successfully detecting all objects.

D. Ablation Studies

To assess the effectiveness of the proposed method, we conduct extensive ablation studies based on our base model, FocusMamba-B on the DSEC-Det dataset.

Contribution of our modules. We take VSS [58] as the base backbone to evaluate the contributions of EGMS, CAE, and FI-Mamba modules. As shown in Tab.III, introducing the three modules progressively provides incremental improvements in both performance and efficiency. Specifically, incorporating the EGMS strategy reduces computation and interference from low-information regions, leading to a 33.1% decrease in FLOPs and a 0.8% increase in mAP. The addition of the CAE module enhances degraded regions in both modalities, increasing mAP by 1.2% without additional computational costs. Finally, integrating FI-Mamba further leverages complementary features across modalities, resulting in another 1.0% improvement in mAP with only a minor computational overhead.

The feature maps before and after the CMFF module are illustrated in Fig.7. CAE module effectively perceives the complementary regions between modalities, as indicated by

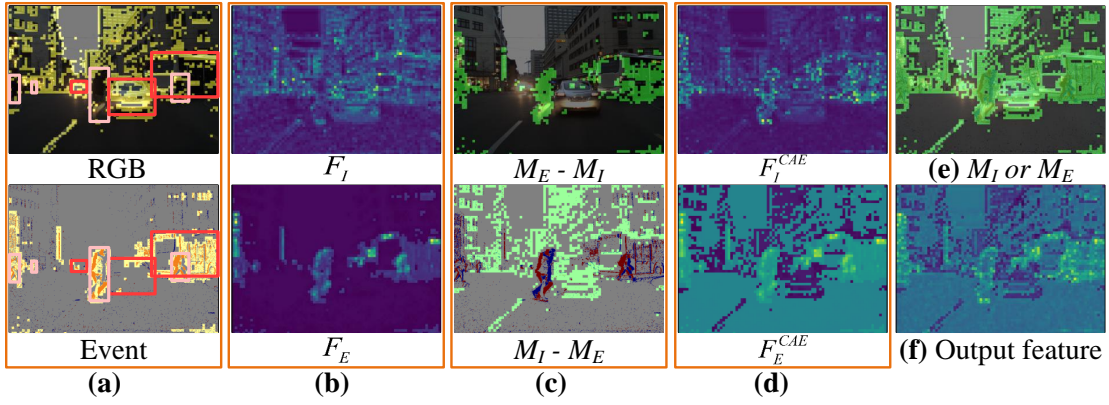


Fig. 7. Visualization of features before and after CMFF module. (a) illustrates the kept regions of the image and event modalities. (c) represents the difference between the kept regions of the two modalities. (b) and (d) present the features before and after the CAE. (e) shows the union of the kept regions from the two modalities. (f) represents the feature after the FI-Mamba.

TABLE IV
PERFORMANCE OF DIFFERENT SCORING METHODS.

Methods	mAP50/mAP	FLOPs	Params
STCA*	52.0/32.2	61.5	44.9
L2 Norm*	50.0/31.6	55.4	44.9
L2 Norm	52.7/32.3	53.6	44.9
SAST	48.9/30.6	51.3	45.6
Ours	55.3/34.6	60.8	44.9

the green regions in Fig.7(c), guiding the image modality to enhance regions with improper exposure and the event modality to suppress low-quality sparse events caused by slow motion, as shown in Fig.7(d). FI-Mamba effectively captures the complementary dependencies between important regions of the two modalities, as shown in Fig.7(e), mitigating background interference and modeling more distinguishable object representations, as shown in Fig.7(f).

Scoring module. To evaluate the effectiveness of our scoring module, we compare it with two joint scoring methods: (1) STCA*: The event modality is scored by the STCA module proposed in [45], and the images use the same score; (2) L2 Norm*: The sum of the two modalities' features is scored based on L2 norm, and the scoring results are shared; and two independent scoring methods: (1) L2 Norm: Scoring each modality independently based on L2 norm; (2) SAST: Scoring each modality independently based on the learning-based scoring module proposed in [44]. As shown in Tab.IV, compared L2 Norm with L2 Norm*, independent scoring outperforms joint scoring under the same metric. This is because joint scoring fails to retain important information for each modality. However, the inaccuracy of the learning-based scoring module in SAST leads to even lower performance than the joint scoring method. Our method, which employs the modality-specific independent scoring strategy, maximizes the strengths of both modalities and achieves superior performance.

The factors in EGCM. We conduct an ablation study to analyze the contribution of the scale factor and control factor in the EGCM. Furthermore, to compare with the fixed kept rate method, we first calculate the average token kept ratios of EGMS and then apply these ratios to remove the same

TABLE V
PERFORMANCE OF THE FACTORS IN EGMS, w/o IS WITHOUT.

Methods	mAP50/mAP	FLOPs
fixed kept rate	53.0/32.8	60.8
w/o scale&control	51.2/31.5	58.6
with scale	53.6/33.3	58.3
with control	52.6/32.6	61.0
with all	55.3/34.6	60.8

TABLE VI
PERFORMANCE OF DIFFERENT FOCUS STRATEGIES IN FI-MAMBA.

Methods	mAP50/mAP	FLOPs
Inter-Mamba	51.3/31.8	63.8
IFI-Mamba	49.0/30.6	59.0
Ours	55.3/34.6	60.8

number of tokens for all samples. As shown in Tab.V, without scale and control factors to regulate the sparsification process, the model lacks scene-adaptive capability, resulting in poor performance. The scale factor facilitates the recognition of informative regions and the filtering of low-information areas, improving accuracy and reducing FLOPs. The control factor directly adjusts the sparsification threshold, enabling the model to adaptively select the number of tokens to retain based on the scene's sparsity, surpassing the fixed kept rate method. Finally, combining both factors achieves a significant performance improvement, providing superior adaptability.

FI-Mamba module. We conduct a comparative analysis of various regional focus strategies in the FI-Mamba module. As shown in Tab.VI, IFI-Mamba which focuses on the intersecting regions of the sparsification maps from both modalities, loses critical information and results in the poorest performance. Inter-Mamba which focuses on all regions, introduces substantial background interference and leads to suboptimal performance. In contrast, our method effectively focuses on the important regions while avoiding background interference, achieving the best performance.

Extension to the ViT-based framework. To validate the broader applicability of EGMS, we integrate it with the ViT-

TABLE VII
PERFORMANCE OF EXTENDING EGMS TO THE ViT-BASED FRAMEWORK.

Methods	mAP50/mAP	FLOPs	Runtime
MaxViT	46.7/29.8	134.7G	60.5ms
MaxViT+EGMS	47.4/30.3	73.4G	45.8ms

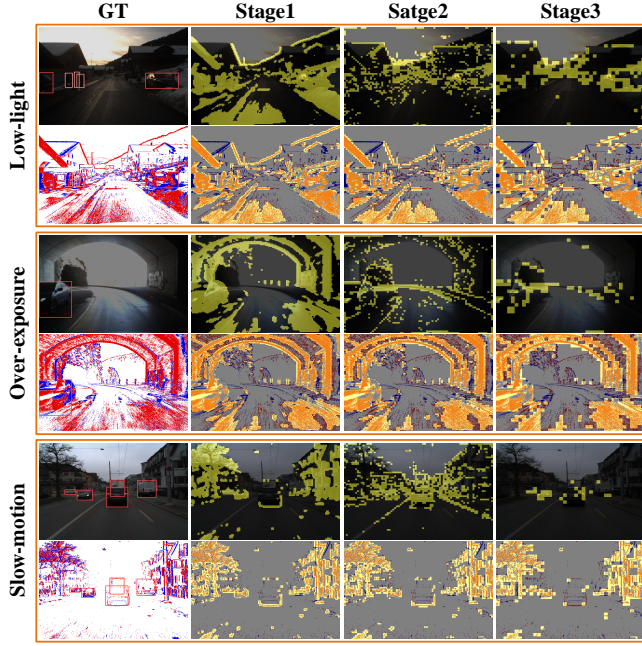


Fig. 8. Visualizations of sparsification results at different stages on the DSEC-Det dataset.

based backbone MaxViT [78] and use simple addition to fuse RGB and event features. As shown in Tab. VII, incorporating EGMS into MaxViT achieves 0.5% gain in mAP and 45.5% reduction in FLOPs on the DSEC-Det dataset, demonstrating the excellent generalization capability of EGMS.

E. Sparsification Visualizations

The sparsification results of the two modalities at different stages on the DSEC-Det and PKU-DAVIS-SOD datasets are shown in Fig. 8 and Fig. 9. Under diverse exposure conditions and scene complexities, our EGMS strategy effectively retains informative tokens (yellow regions) for both modalities, while discarding low-quality tokens, demonstrating robust scene-adaptive capabilities. To be noted that the model primarily focuses on image edges in the early layers, resulting in high feature response magnitudes in edge regions, which leads to a failure in identifying important image tokens. Therefore, to preserve critical information in images, the image modality uses the sparsification map from event modality in stage 1.

Additionally, we assess the scene sparsity by calculating the ratio of triggered event pixels. The relationship between the token kept ratio and the event spatial ratio across the DSEC-Det and PKU-DAVIS-SOD datasets is depicted in Figure 10. The overall trend depicted in the figure indicates that the token kept ratio increases with the event spatial ratio, demonstrating that our method can adaptively perform sparsification based on the scene's sparsity.

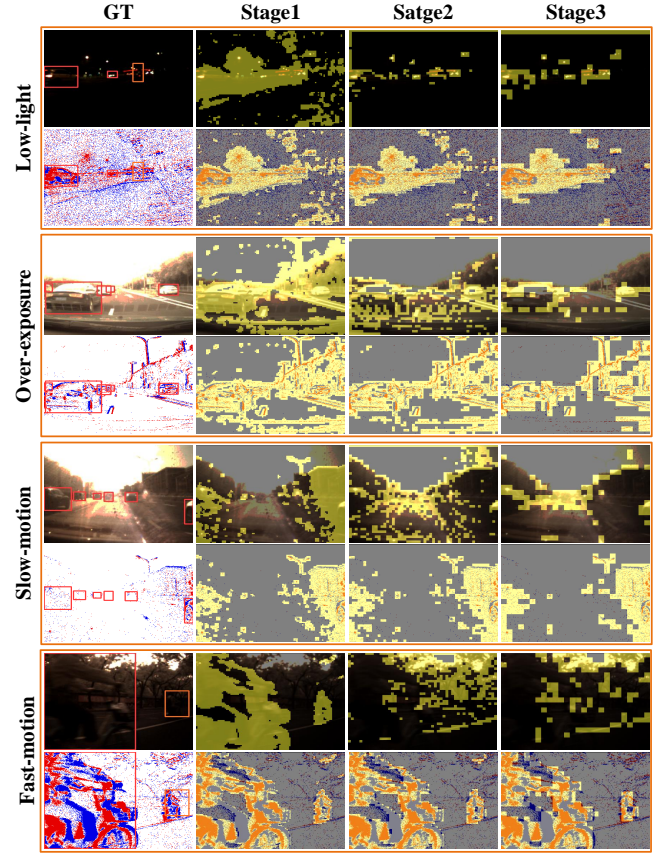


Fig. 9. Visualizations of sparsification results at different stages on the PKU-DAVIS-SOD dataset.

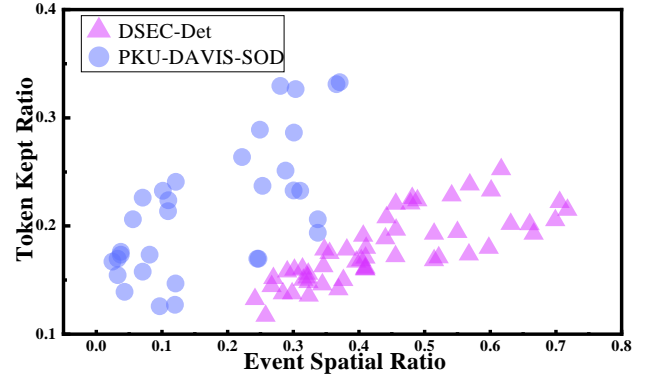


Fig. 10. The trend of the token kept ratio varies with scene sparsity across the DSEC-Det and PKU-DAVIS-SOD datasets. The observed correlation further demonstrates the scene-adaptability of our FocusMamba. Each point represents a sequence.

V. CONCLUSION

In this paper, we propose the FocusMamba which achieves an excellent balance between accuracy and efficiency for RGB-Event based object detection. The EGMS strategy efficiently regulates the token scoring and selection process based on the scene's sparsity level, enabling adaptive retention of critical information and significantly reducing the computational cost. Guided by the sparsification results, the CMFF module effectively perceives and utilizes complementary fea-

tures, eliminating background interference during the fusion process. Experimental results on two datasets demonstrate that our method achieves superior performance.

Limitation. When the scene and the object remain stationary relative to the camera, the event spatial ratio r is difficult to estimate the object information. In such cases, the control factor approaches 1, losing its regulatory effect on the token selection process. To address this limitation, we will incorporate temporal information in future work to enable the propagation of static object information across frames.

REFERENCES

- [1] D. Falanga, K. Kleber, and D. Scaramuzza, “Dynamic obstacle avoidance for quadrotors with event cameras,” *Science Robotics*, vol. 5, no. 40, p. eaaz9712, 2020.
- [2] D. Gehrig and D. Scaramuzza, “Low-latency automotive vision with event cameras,” *Nature*, vol. 629, no. 8014, pp. 1034–1040, 2024.
- [3] Z. Liu, C. Li, N. Yang, Y. Wang, J. Ma, G. Cheng, and X. Zhao, “Mstf: Multiscale transformer for incomplete trajectory prediction,” in *2024 IEEE Intelligent Vehicles Symposium (IV)*. IEEE, 2024, pp. 573–580.
- [4] Z. Liu, J. Cheng, J. Fan, S. Lin, Y. Wang, and X. Zhao, “Multi-modal fusion based on depth adaptive mechanism for 3d object detection,” *IEEE Transactions on Multimedia*, vol. 27, pp. 707–717, 2023.
- [5] C. Li, Z. Liu, S. Lin, Y. Wang, and X. Zhao, “Intention-convolution and hybrid-attention network for vehicle trajectory prediction,” *Expert Systems with Applications*, vol. 236, p. 121412, 2024.
- [6] C. Li, Z. Liu, N. Yang, W. Li, and X. Zhao, “Regional attention network with data-driven modal representation for multimodal trajectory prediction,” *Expert Systems with Applications*, vol. 232, p. 120808, 2023.
- [7] L. Peng, Y. Cao, Y. Sun, and Y. Wang, “Lightweight adaptive feature de-drifting for compressed image classification,” *IEEE Transactions on Multimedia*, vol. 26, pp. 6424–6436, 2024.
- [8] Z. Liu, M. Qi, C. Shen, Y. Fang, and X. Zhao, “Cascade saccade machine learning network with hierarchical classes for traffic sign detection,” *Sustainable Cities and Society*, vol. 67, p. 102700, 2021.
- [9] X. Zhao, M. Qi, Z. Liu, S. Fan, C. Li, and M. Dong, “End-to-end autonomous driving decision model joined by attention mechanism and spatiotemporal features,” *IET intelligent transport systems*, vol. 15, no. 9, pp. 1119–1130, 2021.
- [10] Z. Liu, C. Li, Y. Wang, N. Yang, X. Fan, J. Ma, and X. Zhao, “Multi-scale temporal fusion transformer for incomplete vehicle trajectory prediction,” *IEEE Transactions on Intelligent Vehicles*, 2024.
- [11] S. Kuang, Y. Liu, X. Wang, X. Wu, and Y. Wei, “Harnessing multimodal large language models for traffic knowledge graph generation and decision-making,” p. 100146, 2024.
- [12] X. Qu, H. Lin, and Y. Liu, “Envisioning the future of transportation: Inspiration of chatgpt and large models,” p. 100103, 2023.
- [13] C. Li, Z. Liu, J. Zhang, Y. Wang, F. Ding, and X. Zhao, “Two-stream lstm network with hybrid attention for vehicle trajectory prediction,” in *2022 IEEE 25th International Conference on Intelligent Transportation Systems (ITSC)*. IEEE, 2022, pp. 1927–1934.
- [14] L. Peng, Y. Wang, X. Di, X. Fu, Y. Cao, Z.-J. Zha *et al.*, “Boosting image de-raining via central-surrounding synergistic convolution,” in *Proceedings of the AAAI Conference on Artificial Intelligence*, vol. 39, no. 6, 2025, pp. 6470–6478.
- [15] L. Peng, A. Wu, W. Li, P. Xia, X. Dai, X. Zhang, X. Di, H. Sun, R. Pei, Y. Wang *et al.*, “Pixel to gaussian: Ultra-fast continuous super-resolution with 2d gaussian modeling,” *arXiv preprint arXiv:2503.06617*, 2025.
- [16] Z. Liu, N. Yang, Y. Wang, Y. Li, X. Zhao, and F.-Y. Wang, “Enhancing traffic object detection in variable illumination with rgb-event fusion,” *IEEE Transactions on Intelligent Transportation Systems*, 2024.
- [17] Z. Liu, Y. Li, Y. Wang, B. Gao, Y. An, and X. Zhao, “Boosting visual recognition in real-world degradations via unsupervised feature enhancement module with deep channel prior,” *IEEE Transactions on Intelligent Vehicles*, 2024.
- [18] Y. Wang, J. Zhang, Y. Cao, and Z. Wang, “A deep cnn method for underwater image enhancement,” in *2017 IEEE international conference on image processing (ICIP)*. IEEE, 2017, pp. 1382–1386.
- [19] Y. Wang, L. Peng, L. Li, Y. Cao, and Z.-J. Zha, “Decoupling-and-aggregating for image exposure correction,” in *Proceedings of the IEEE/CVF conference on computer vision and pattern recognition*, 2023, pp. 18 115–18 124.
- [20] L. Peng, Y. Cao, R. Pei, W. Li, J. Guo, X. Fu, Y. Wang, and Z.-J. Zha, “Efficient real-world image super-resolution via adaptive directional gradient convolution,” *arXiv preprint arXiv:2405.07023*, 2024.
- [21] H. Wang, L. Peng, Y. Sun, Z. Wan, Y. Wang, and Y. Cao, “Brightness perceiving for recursive low-light image enhancement,” *IEEE Transactions on Artificial Intelligence*, vol. 5, no. 6, pp. 3034–3045, 2023.
- [22] A. Wu, L. Peng, X. Di, X. Dai, C. Wu, Y. Wang, X. Fu, Y. Cao, and Z.-J. Zha, “Robustgs: Unified boosting of feedforward 3d gaussian splatting under low-quality conditions,” *arXiv preprint arXiv:2508.03077*, 2025.
- [23] Y. Wang, Y. Cao, Z.-J. Zha, J. Zhang, and Z. Xiong, “Deep degradation prior for low-quality image classification,” in *Proceedings of the IEEE/CVF Conference on Computer Vision and Pattern Recognition*, 2020, pp. 11 049–11 058.
- [24] G. Gallego, T. Delbrück, G. Orchard, C. Bartolozzi, B. Taba, A. Censi, S. Leutenegger, A. J. Davison, J. Conradt, K. Daniilidis *et al.*, “Event-based vision: A survey,” *IEEE transactions on pattern analysis and machine intelligence*, vol. 44, no. 1, pp. 154–180, 2020.
- [25] S. Ding, J. Chen, Y. Wang, Y. Kang, W. Song, J. Cheng, and Y. Cao, “E-mlb: Multilevel benchmark for event-based camera denoising,” *IEEE Transactions on Multimedia*, vol. 26, pp. 65–76, 2023.
- [26] L. Peng, W. Li, J. Guo, X. Di, H. Sun, Y. Li, R. Pei, Y. Wang, Y. Cao, and Z.-J. Zha, “Unveiling hidden details: A raw data-enhanced paradigm for real-world super-resolution,” *arXiv preprint arXiv:2411.10798*, 2024.
- [27] G. Tan, Y. Wang, H. Han, Y. Cao, F. Wu, and Z.-J. Zha, “Multi-grained spatio-temporal features perceived network for event-based lip-reading,” in *Proceedings of the IEEE/CVF Conference on Computer Vision and Pattern Recognition*, 2022, pp. 20 094–20 103.
- [28] Z. Wan, G. Tan, Y. Wang, W. Zhai, Y. Cao, and Z.-J. Zha, “Event-based optical flow via transforming into motion-dependent view,” *IEEE Transactions on Image Processing*, vol. 33, pp. 5327–5339, 2024.
- [29] J. Chen, Y. Wang, Y. Cao, F. Wu, and Z.-J. Zha, “Progressivemotionseg: Mutually reinforced framework for event-based motion segmentation,” in *Proceedings of the AAAI Conference on Artificial Intelligence*, vol. 36, no. 1, 2022, pp. 303–311.
- [30] Y. Wang, Y. Cao, Z.-J. Zha, J. Zhang, Z. Xiong, W. Zhang, and F. Wu, “Progressive retinex: Mutually reinforced illumination-noise perception network for low-light image enhancement,” in *Proceedings of the 27th ACM international conference on multimedia*, 2019, pp. 2015–2023.
- [31] B. Xie, Y. Deng, Z. Shao, Q. Xu, and Y. Li, “Event voxel set transformer for spatiotemporal representation learning on event streams,” *IEEE Transactions on Circuits and Systems for Video Technology*, 2024.
- [32] Z. Chen, J. Wu, J. Hou, L. Li, W. Dong, and G. Shi, “Ecsnet: Spatio-temporal feature learning for event camera,” *IEEE Transactions on Circuits and Systems for Video Technology*, vol. 33, no. 2, pp. 701–712, 2022.
- [33] D. Liu, T. Wang, and C. Sun, “Voxel-based multi-scale transformer network for event stream processing,” *IEEE Transactions on Circuits and Systems for Video Technology*, vol. 34, no. 4, pp. 2112–2124, 2023.
- [34] D. Li, Y. Tian, and J. Li, “Sodformer: Streaming object detection with transformer using events and frames,” *IEEE Transactions on Pattern Analysis and Machine Intelligence*, vol. 45, no. 11, pp. 14 020–14 037, 2023.
- [35] X. Long, X. Zhu, F. Guo, C. Chen, X. Zhu, F. Gu, S. Yuan, and C. Zhang, “Spike-brgnet: Efficient and accurate event-based semantic segmentation with boundary region-guided spiking neural networks,” *IEEE Transactions on Circuits and Systems for Video Technology*, 2024.
- [36] Z. Liu, Y. Sun, Y. Wang, N. Yang, S. E. Li, and X. Zhao, “Beyond conventional vision: Rgb-event fusion for robust object detection in dynamic traffic scenarios,” *Communications in Transportation Research*, vol. 5, p. 100202, 2025.
- [37] X. Liu, J. Li, J. Shi, X. Fan, Y. Tian, and D. Zhao, “Event-based monocular depth estimation with recurrent transformers,” *IEEE Transactions on Circuits and Systems for Video Technology*, vol. 34, no. 8, pp. 7417–7429, 2024.
- [38] A. Tomy, A. Paigwar, K. S. Mann, A. Renzaglia, and C. Laugier, “Fusing event-based and rgb camera for robust object detection in adverse conditions,” in *2022 International Conference on Robotics and Automation (ICRA)*. IEEE, 2022, pp. 933–939.
- [39] N. Yang, Z. Liu, S. Ma, Y. Sun, Y. He, and Y. Wang, “Joint intensity and event framework for vehicle detection in degraded conditions,” in *2023 7th International Conference on Transportation Information and Safety (ICTIS)*. IEEE, 2023, pp. 1568–1574.
- [40] J. Cao, X. Zheng, Y. Lyu, J. Wang, R. Xu, and L. Wang, “Chasing day and night: Towards robust and efficient all-day object detection guided by an event camera,” in *2024 IEEE International Conference on Robotics and Automation (ICRA)*. IEEE, 2024, pp. 9026–9032.

- [41] B. Roh, J. Shin, W. Shin, and S. Kim, "Sparse detr: Efficient end-to-end object detection with learnable sparsity," *arXiv preprint arXiv:2111.14330*, 2021.
- [42] X. Liu, T. Wu, and G. Guo, "Adaptive sparse vit: Towards learnable adaptive token pruning by fully exploiting self-attention," *arXiv preprint arXiv:2209.13802*, 2022.
- [43] Y. Liu, M. Gehrig, N. Messikommer, M. Cannici, and D. Scaramuzza, "Revisiting token pruning for object detection and instance segmentation," in *Proceedings of the IEEE/CVF Winter Conference on Applications of Computer Vision*, 2024, pp. 2658–2668.
- [44] Y. Peng, H. Li, Y. Zhang, X. Sun, and F. Wu, "Scene adaptive sparse transformer for event-based object detection," in *Proceedings of the IEEE/CVF Conference on Computer Vision and Pattern Recognition*, 2024, pp. 16 794–16 804.
- [45] N. Yang, Y. Wang, Z. Liu, M. Li, Y. An, and X. Zhao, "Smamba: Sparse mamba for event-based object detection," *arXiv preprint arXiv:2501.11971*, 2025.
- [46] X. Chen, Z. Liu, H. Tang, L. Yi, H. Zhao, and S. Han, "Sparsevit: Revisiting activation sparsity for efficient high-resolution vision transformer," in *Proceedings of the IEEE/CVF Conference on Computer Vision and Pattern Recognition*, 2023, pp. 2061–2070.
- [47] Z. Zhou, Z. Wu, R. Bouteau, F. Yang, C. Demonceaux, and D. Ginjac, "Rgb-event fusion for moving object detection in autonomous driving," *arXiv preprint arXiv:2209.08323*, 2022.
- [48] H. Cao, Z. Zhang, Y. Xia, X. Li, J. Xia, G. Chen, and A. Knoll, "Embracing events and frames with hierarchical feature refinement network for object detection," in *European Conference on Computer Vision*. Springer, 2025, pp. 161–177.
- [49] L. Xing, Q. Huang, X. Dong, J. Lu, P. Zhang, Y. Zang, Y. Cao, C. He, J. Wang, F. Wu *et al.*, "Pyramidrop: Accelerating your large vision-language models via pyramid visual redundancy reduction," *arXiv preprint arXiv:2410.17247*, 2024.
- [50] L. Chen, H. Zhao, T. Liu, S. Bai, J. Lin, C. Zhou, and B. Chang, "An image is worth 1/2 tokens after layer 2: Plug-and-play inference acceleration for large vision-language models," in *European Conference on Computer Vision*. Springer, 2024, pp. 19–35.
- [51] W. Ye, Q. Wu, W. Lin, and Y. Zhou, "Fit and prune: Fast and training-free visual token pruning for multi-modal large language models," in *Proceedings of the AAAI Conference on Artificial Intelligence*, vol. 39, no. 21, 2025, pp. 22 128–22 136.
- [52] M. Dhoubi, D. Buscaldi, S. Vanier, and A. Shabou, "Pact: Pruning and clustering-based token reduction for faster visual language models," *arXiv preprint arXiv:2504.08966*, 2025.
- [53] Z. Lin, M. Lin, L. Lin, and R. Ji, "Boosting multimodal large language models with visual tokens withdrawal for rapid inference," in *Proceedings of the AAAI Conference on Artificial Intelligence*, vol. 39, no. 5, 2025, pp. 5334–5342.
- [54] Y. Rao, W. Zhao, B. Liu, J. Lu, J. Zhou, and C.-J. Hsieh, "Dynamicvit: Efficient vision transformers with dynamic token sparsification," *Advances in neural information processing systems*, vol. 34, pp. 13 937–13 949, 2021.
- [55] Z. Kong, P. Dong, X. Ma, X. Meng, W. Niu, M. Sun, X. Shen, G. Yuan, B. Ren, H. Tang *et al.*, "Svit: Enabling faster vision transformers via latency-aware soft token pruning," in *European conference on computer vision*. Springer, 2022, pp. 620–640.
- [56] A. Gu and T. Dao, "Mamba: Linear-time sequence modeling with selective state spaces," *arXiv preprint arXiv:2312.00752*, 2023.
- [57] L. Zhu, B. Liao, Q. Zhang, X. Wang, W. Liu, and X. Wang, "Vision mamba: Efficient visual representation learning with bidirectional state space model," *arXiv preprint arXiv:2401.09417*, 2024.
- [58] Y. Liu, Y. Tian, Y. Zhao, H. Yu, L. Xie, Y. Wang, Q. Ye, and Y. Liu, "Vmamba: Visual state space model," *arXiv preprint arXiv:2401.10166*, 2024.
- [59] R. Xu, S. Yang, Y. Wang, B. Du, and H. Chen, "A survey on vision mamba: Models, applications and challenges," *arXiv preprint arXiv:2404.18861*, 2024.
- [60] B. N. Patro and V. S. Agneeswaran, "Mamba-360: Survey of state space models as transformer alternative for long sequence modelling: Methods, applications, and challenges," *arXiv preprint arXiv:2404.16112*, 2024.
- [61] Z. Wan, P. Zhang, Y. Wang, S. Yong, S. Stepputtis, K. Sycara, and Y. Xie, "Sigma: Siamese mamba network for multi-modal semantic segmentation," *arXiv preprint arXiv:2404.04256*, 2024.
- [62] H. Guo, J. Li, T. Dai, Z. Ouyang, X. Ren, and S.-T. Xia, "Mambair: A simple baseline for image restoration with state-space model," in *ECCV*, 2024.
- [63] W. Zou, H. Gao, W. Yang, and T. Liu, "Wave-mamba: Wavelet state space model for ultra-high-definition low-light image enhancement," in *ACM Multimedia 2024*, 2024.
- [64] J. Huang, S. Wang, S. Wang, Z. Wu, X. Wang, and B. Jiang, "Mamba-ftrack: Frame-event tracking via state space model," in *Chinese Conference on Pattern Recognition and Computer Vision (PRCV)*. Springer, 2024, pp. 3–18.
- [65] L. Peng, X. Di, Z. Feng, W. Li, R. Pei, Y. Wang, X. Fu, Y. Cao, and Z.-J. Zha, "Directing mamba to complex textures: An efficient texture-aware state space model for image restoration," *arXiv preprint arXiv:2501.16583*, 2025.
- [66] X. Di, L. Peng, P. Xia, W. Li, R. Pei, Y. Cao, Y. Wang, and Z.-J. Zha, "Qmambabsr: Burst image super-resolution with query state space model," in *Proceedings of the Computer Vision and Pattern Recognition Conference*, 2025, pp. 23 080–23 090.
- [67] A. Z. Zhu, L. Yuan, K. Chaney, and K. Daniilidis, "Unsupervised event-based learning of optical flow, depth, and egomotion," in *Proceedings of the IEEE/CVF Conference on Computer Vision and Pattern Recognition*, 2019, pp. 989–997.
- [68] H. Chefer, S. Gur, and L. Wolf, "Transformer interpretability beyond attention visualization," in *Proceedings of the IEEE/CVF conference on computer vision and pattern recognition*, 2021, pp. 782–791.
- [69] B. Wu, C. Xu, X. Dai, A. Wan, P. Zhang, Z. Yan, M. Tomizuka, J. Gonzalez, K. Keutzer, and P. Vajda, "Visual transformers: Token-based image representation and processing for computer vision," *arXiv preprint arXiv:2006.03677*, 2020.
- [70] Y. He, G. Kang, X. Dong, Y. Fu, and Y. Yang, "Soft filter pruning for accelerating deep convolutional neural networks," in *International Joint Conference on Artificial Intelligence (IJCAI)*, 2018, pp. 2234–2240.
- [71] T.-Y. Lin, M. Maire, S. Belongie, J. Hays, P. Perona, D. Ramanan, P. Dollár, and C. L. Zitnick, "Microsoft coco: Common objects in context," in *Computer Vision—ECCV 2014: 13th European Conference, Zurich, Switzerland, September 6–12, 2014, Proceedings, Part V 13*. Springer, 2014, pp. 740–755.
- [72] N. Zubic, M. Gehrig, and D. Scaramuzza, "State space models for event cameras," in *Proceedings of the IEEE/CVF Conference on Computer Vision and Pattern Recognition*, 2024, pp. 5819–5828.
- [73] Z. Ge, S. Liu, F. Wang, Z. Li, and J. Sun, "Yolox: Exceeding yolo series in 2021," *arXiv preprint arXiv:2107.08430*, 2021.
- [74] R. Khanam and M. Hussain, "Yolov11: An overview of the key architectural enhancements," *arXiv preprint arXiv:2410.17725*, 2024.
- [75] Z. Wang, C. Li, H. Xu, and X. Zhu, "Mamba yolo: Ssms-based yolo for object detection," *arXiv preprint arXiv:2406.05835*, 2024.
- [76] D. Li, J. Li, X. Liu, X. Fan, and Y. Tian, "Asynchronous collaborative graph representation for frames and events," in *Proceedings of the Computer Vision and Pattern Recognition Conference*, 2025, pp. 1655–1666.
- [77] S. R. Alvar, G. Singh, M. Akbari, and Y. Zhang, "Divprune: Diversity-based visual token pruning for large multimodal models," *arXiv preprint arXiv:2503.02175*, 2025.
- [78] Z. Tu, H. Talebi, H. Zhang, F. Yang, P. Milanfar, A. Bovik, and Y. Li, "Maxvit: Multi-axis vision transformer," in *European conference on computer vision*. Springer, 2022, pp. 459–479.